Granula Motion and Membrane Spreading During Activation of Human Platelets Imaged by Atomic Force Microscopy

Monika Fritz, Manfred Radmacher, and Hermann E. Gaub
Physik-Department, Lehrstuhl für Biophysik, Technische Universität München, 85748 Garching, Germany

ABSTRACT The redistribution of platelet constituents during activation is essential for their physiological function of maintaining hemostasis. We report here about real time investigations of the activation of native human platelets under physiological conditions from the initial formation of filopodia to the fully spread form by atomic force microscopy. We followed the trafficking of granules and their interaction with the plasma membrane within single cells. Our results show movement of certain granula towards the lamellipodia. Analysis of this rearrangement and the subsequent enlargement of the platelet surface reveals details of the membrane spreading process. Images of living cells are presented that show the distribution of cytoskeletal components and membrane-bound filaments at a resolution of better than 50 nm. The local minimum forces between the tip and the platelets were estimated to be smaller than 60 pN. A model for the elastic contributions of the glycocalix to the tip/membrane interaction was developed using the theory of grafted polymers.

INTRODUCTION

Platelets are anucleated blood cells whose function is to maintain the integrity of blood vessels by adhering to injuries, and subsequently activating essential steps in blood clotting (Behnke, 1976). During activation platelets undergo a drastic shape change from a discoid form about 3 μm in diameter to a flat spread form 7–10 μm in diameter (Allen et al., 1979). This is necessitated by the two extremes of their physiological functions: in the resting stage platelets must resist blood pressure without sticking together, whereas during activation they must initiate aggregation. This response is a very complex process, including redistribution of granula, spreading and enlargement of the surface area, and a reorganization of the whole cytoskeleton. As contractile motors, platelets together with fibrin are responsible for the clot retraction. In the resting discoid form platelets contain a large number of vesicles (granula) and membrane tubules. During the activation process, after stimulation by agonists such as thrombin, ADP, or a foreign wettable surface, certain vesicles fuse with the plasma membrane. These vesicles secrete chemical substances and increase the surface area of the platelet (Ginsberg et al., 1980; Holmsen, 1980). Another population of vesicles, concentrated in the center of the cell, forms the granulomer or pseudonucleus (Morgenstern and Kho, 1977; White and Krumwiede, 1987). Platelets can secrete their granules either by an invagination of the plasma membrane—the open canalicular system (OCS) (Stenberg et al., 1984)—or directly by fusion with the plasma membrane (White, 1987). Activation of platelets is accompanied by a drastic reorganization of the cytoskeleton. The microtubule ring in the resting platelet disassembles and the pool of capped monomeric actin polymerizes, forming a tight actin filament network (Hartwig and DeSisto, 1991; Loftus et al., 1984; Nachmias, 1980). Together with myosin these filaments form a contractile cytoskeleton (Sixma et al., 1989). In this study, redistribution of granula during activation of individual platelets on a cover glass was investigated by atomic force microscopy (AFM).

Although designed for atomic lattice imaging (Binnig et al., 1986), the AFM has recently proven to be an extremely powerful instrument for the investigation of live cells (Henderson et al., 1992; Keller et al., 1992; Radmacher et al., 1992b). The major advantage of this novel and largely noninvasive microscopy is the capability of recording dynamic processes with an unparalleled spatial resolution (Fritz et al., 1993; Häberle et al., 1992). The AFM scans the surface of the sample with a sharp tip at the end of a soft cantilever (Fig. 1). At low scanning forces the image is dominated by the surface relief, whereas at higher forces the local elasticity contributes significantly, so that internal structures such as the cytoskeleton become visible. Plots of force versus sample height on the cells show that no net force between the tip and the sample was detectable. This may be explained by the elastic properties of the cell membrane, especially the glycocalix.

Received for publication 4 October 1993 and in final form 3 February 1994.

Address reprint requests to Hermann E. Gaub, Physik-Department, Lehrstuhl für Biophysik, E22, Technische Universität München, 85748 Garching, Germany.

Dr. Fritz's present address: Marine Science Institute, University of California, Santa Barbara, CA 93106 USA.

Dr. Radmacher's present address: Department of Physics, University of California, Santa Barbara, CA 93106 USA.

0006-3495/94/05/1328/07 $2.00

MATERIAL AND METHODS

Platelet preparation

Fresh human platelet concentrate was obtained from the Bayerisches Rotes Kreuz (München). The platelets were suspended in acid-citrate-dextrose anticoagulant solution (18 mM dextrose, 8 mM Na_3-citrate, 5.2 mM citric acid) and stored at room temperature. Immediately before the experiment, the platelets were centrifuged at 100 × *g* for 10 min at room temperature. The pellet was resuspended in HEPES Tyrode buffer (3 mM HEPES, 4 mM NaH_2PO_4, 137 mM NaCl, 2.6 mM KCl, 1 mM $MgCl_2$, pH 7.3) to a final

concentration of 10^5 platelets/μl. The platelets were allowed to adhere to glass cover slips for 30 s at room temperature before imaging.

Instrumentation

AFM images were recorded with a combined fluorescence/force microscope built in our laboratory (Radmacher et al., 1992a). To show both the large scale height profile of the cells and the fine corrugations on the surface, the images were recorded in the error-signal mode (Putman et al., 1992). In this mode the large cantilever deflection is compensated through feedback control of sample height resulting in the height image. The remaining deflection signal is amplified and recorded, giving the fine corrugation image (see Fig. 1). These images are presented either in parallel or are summed after contrast calibration to form a single image. Commercially available silicon nitride cantilevers (Digital Instruments, Santa Barbara, CA; nominal spring constant 32 mN/m) with integrated tips were used (for the measurement of spring constants see Cleveland et al., 1993). The radius of curvature of such tips is typically 30 nm. The tips were cleaned before imaging by argon-plasma discharge in a commercially available plasma cleaner (PDC-3XG, Harrick, Ossining, NY).

RESULTS AND DISCUSSION

Activation of platelets on glass surfaces

Fig. 2 shows a time course of the activation of a human platelet on glass. The first step of activation is not accessible with our instrument, because platelets in their resting stage do not adhere well enough to glass cover slides for stable imaging. In *A* the nearly discoid platelet with some filopodia begins to adhere to the substrate. In the beginning the filopodia appear to be spike-like protrusions (*A*, *red* and *blue arrows*). The extra membrane needed for these filopodia is generally believed to be provided by a fast extrusion of the OCS from the inside of the cell (White, 1983). In the next step granula appear at the cortex of the cell (*B, C*, *green* and *blue arrows*). In *B* a large, flat lamellipodium is formed (*red arrow*) between the protrusions, which is free of granula. One minute later in *C* the large, flat lamellipodium is filled with granules (*red arrow*) and two filopodia (*B*, *blue arrow*) have fused to form a granula-filled lamellipodium. During the sequence (*B–F*) some granula move towards the cortex and vanish while the area of the cell increases (*green* and *blue arrows*). Our observations support the idea that during activation granula fuse directly with the plasma membrane (Morgenstern et al., 1987; Zucker-Franklin et al., 1985). At the time image *E* is recorded, the shape change is nearly complete: a few granula remain distributed over the lamellipodia (*red* and *green arrows*). Those granula gradually fade (*F*, *red* and *blue arrows*) and have disappeared by *G*. In *H* rough cytoskeletal structures are visible (*green arrow*). The activation may be summarized as follows: thin filopodia protrude from the interior of the platelet and are then filled with granula that come from the center of the cell eventually forming a flat lamellipodium. In addition to the findings of other groups (Behnke and Bray, 1988; White, 1983) who have reported an inward flow of the granula, our data clearly demonstrate that a significant number of granula are transported towards the cortex.

Further observations, shown in Fig. 3, support the conclusion of direct fusion of granula with the plasma membrane. Fig. 3 gives a detailed view on the activation of a platelet at the stage comparable to the stage in Fig. 2 *D*. The membrane creeps towards the upper left corner (*black arrows*) while the fiber (*blue arrows*) remains nearly stationary. In this detailed view, the attachment of the membrane to the glass substrate appears to be a discontinous process where little membrane fingers adhere to the glass in a wetting-like process probably supported by a transient cytoskeletal network (Evans, 1993) (*arrow*). In contrast to the cytoskeletal structures visible in Fig. 5, this fiber shows sharp contrast in the AFM image, which indicates that this fiber is attached to the outside of the cell.

Investigations by scanning electron microscopy have shown that fibrin strands bind approximately 15 nm from the platelet surface (Morgenstern et al., 1984), so that they stick out of the glycocalix. This may be the reason for the sharp contrast in Fig. 4. Fig. 4 *A* shows the small corrugations on the cell surface, with several filaments running in parallel over a long distance following contours of intracellular organelles. They are also visible in the height image (Fig. 4 *B*).

Once the redistribution processes have abated and the lamellipodia have degranulated, the cytoskeleton of the platelets may be imaged. Fig. 5 shows a platelet in the fully activated stage. In *A* the entire platelet is scanned. The accumulation of granula in the center that form the pseudonucleus is clearly visible. As was previously demonstrated by Loftus et al. (1984) in a transmission electron microscope study, the cytoskeleton of the activated platelet was divided into four structurally distinct zones: the cortex

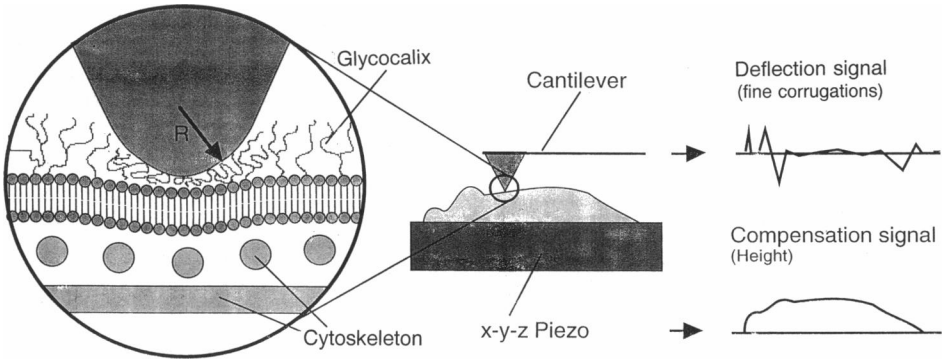

FIGURE 1 Schematics of our AFM and the signals measured in imaging cells (*right-hand side*). The deflection of the cantilever is compensated by adjusting the vertical sample position resulting in the height image. The remaining deflection signal is amplified giving the fine corrugation image. The close-up view (*left-hand side*) sketches the interactions between tip and cell membrane mainly the elastic interactions of glycocalix, membrane and the underlying cytoskeleton.

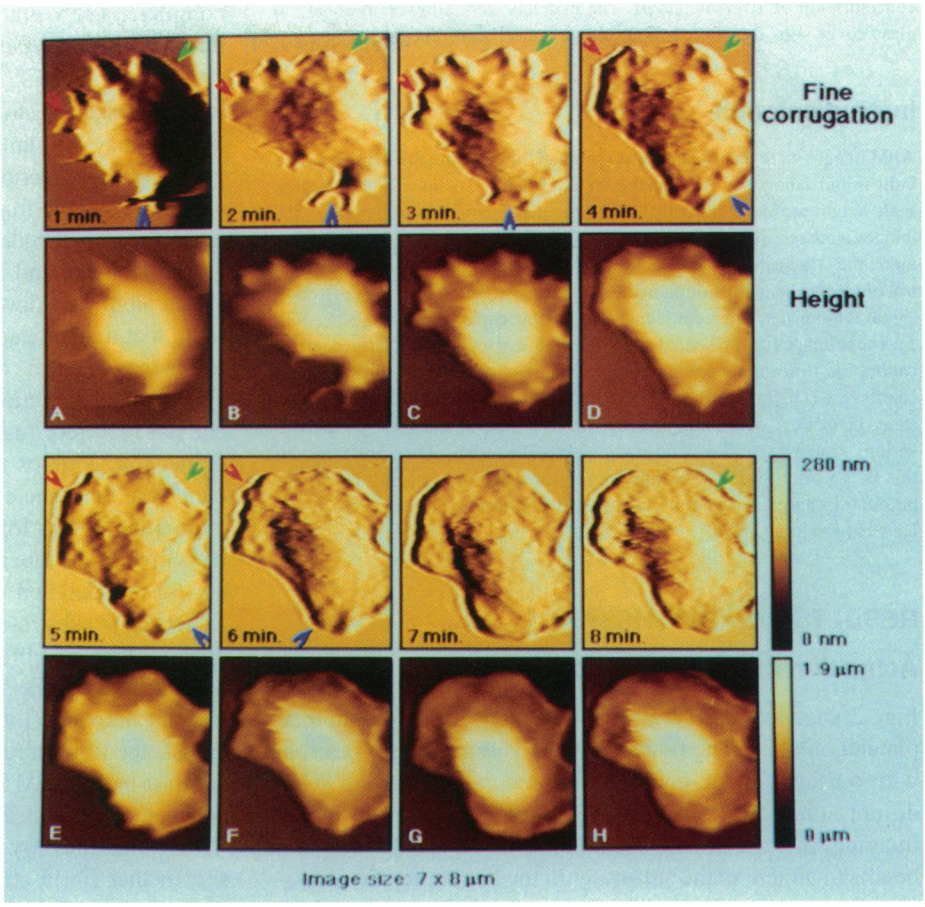

FIGURE 2 Time-series of the activation of a human platelet on glass imaged with the AFM. Images *A–H* show a complete sequence of the activation on glass. Images in the upper row show the small corrugations on the cell surface, images below show the large corrugations (height). A detailed description is given in the text.

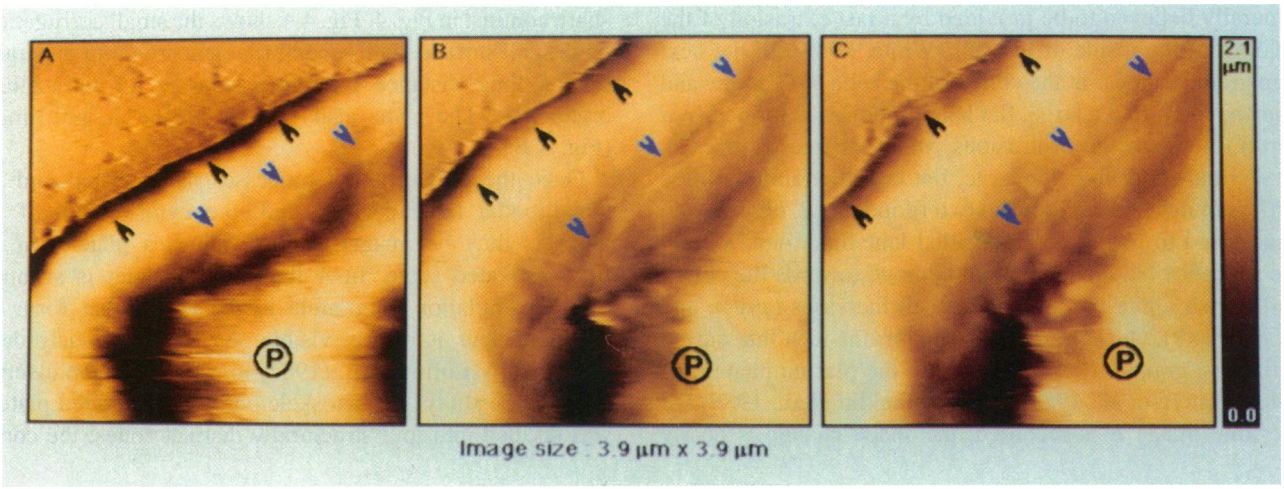

FIGURE 3 Magnified view of the cortex movement during platelet activation. The three images (*A–C*) were recorded at 40-s intervals. The parallel images of the error signal mode were contrast-calibrated and summed. The cortex (*black arrows*) creeps over the cover glass while the pseudonucleus (P) remains stationary. A filament (*blue arrows*) is bound to the outside of the membrane between the cortex and the pseudonucleus. During the movement of the cortex the filament remains nearly stationary with respect to the pseudonucleus (*black* and *blue arrows*).

or peripheral web (W), the outer filamentous zone (O), the inner filamentous zone (I), and in the center of the cell, the granulomer (P). The cortex of the cell is a tight network of short filaments that are capped mainly by gelsolin (Hartwig, 1992). These filaments, which apparently consist only of microfilaments, are so densely packed that the AFM tip cannot resolve them. The outer filamentous zone consists of loosely packed microfilament bundles (20–40 nm in diameter) and microtubules (about 25 nm in diameter). These filaments are oriented parallel and normal to the cell cortex. Bundles of these filaments or even single filaments can be imaged by the AFM (O). The inner fila-

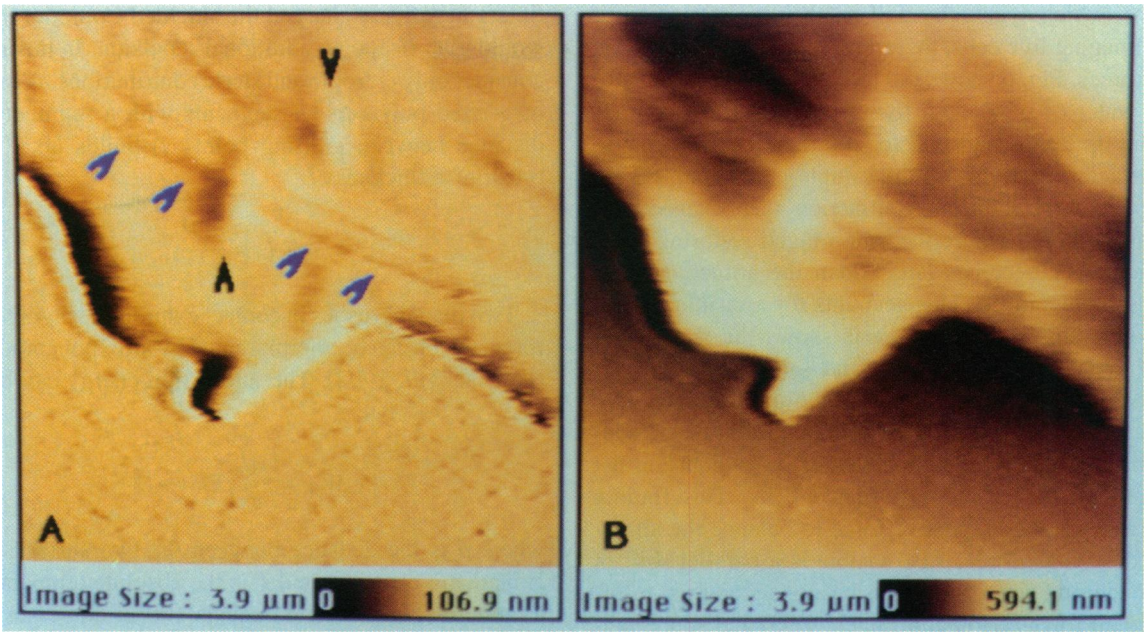

FIGURE 4 Lamellipodium of an activating platelet. The image *A* shows the small corrugations, the image *B* the height. Clearly visible are two organelles (*black arrows*) and filament bundles attached to the surface (*blue arrows*) of the platelet lamellipodium. The fiber bundles run over the organelle following its contours.

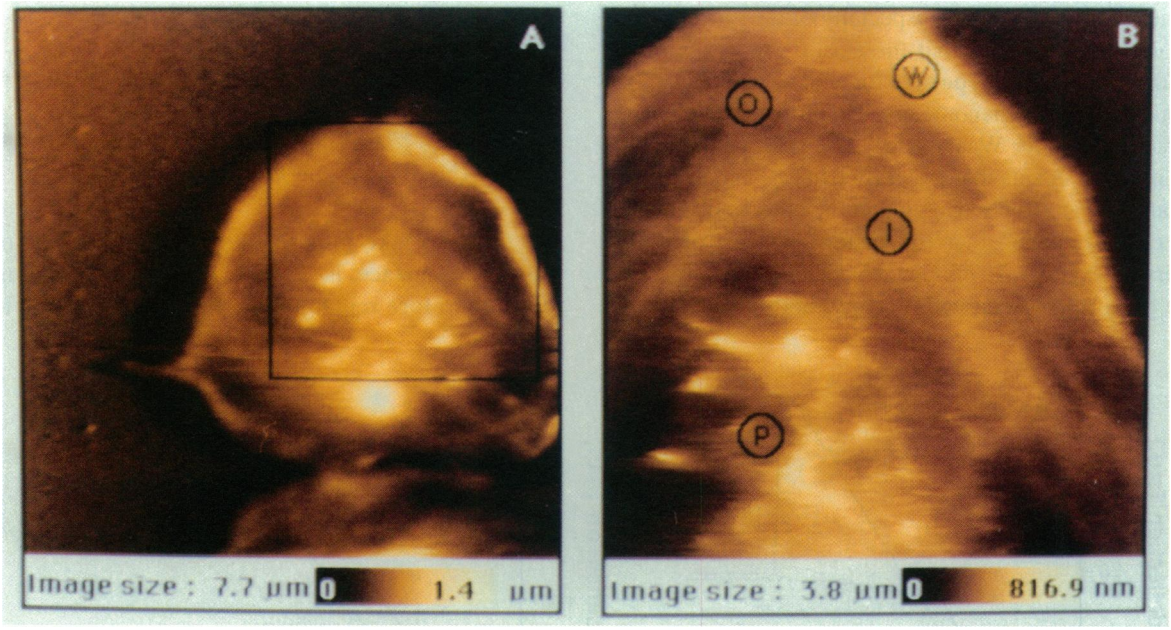

FIGURE 5 Platelet in the fully activated stage. The parallel images of the error signal mode were contrast-calibrated and added. In (*A*) the entire platelet is scanned. Clearly visible are the granules that form the pseudonucleus. In (*B*) (rectangle in *A*) the four structurally distinct zones of activated platelets are clearly visible and labeled: The cortex or peripheral web (W), the outer filamentous zone (O), the inner filamentous zone (I) and, in the center of the cell, the granulomer (P). The lamellipodia are completely degranulated.

mentous zone is a more densely packed structure. The filament network consists of discrete overlapping actin polymers and myosin to form the contractile part of the cytoskeleton (Painter and Ginsberg, 1981; Pollard et al., 1977). Fig. 5 demonstrates that these four zones are also clearly distinguishable in intact, living platelets that have not undergone fixation or extraction of triton-soluble material (see characters in *B*). In a parallel study we have shown that the peripheral web (W) consists of Cytochalasin B degradable actin filaments (Fritz et al., 1994).

Forces in imaging

Imaging by AFM involves forces between tip and sample. It is obvious that at high forces the tip may penetrate the cell

membrane, which eventually will result in a destruction of the cell. Imaging live cells, therefore, requires minimization of these forces. Fig. 6 shows the force curve on a glass substrate in water (*A*) and on a living platelet (*B*). Upon approach the tip jumps into contact and then follows the rise of the surface (Fig. 6 *A*). As the sample is lowered, the tip stays trapped in the short range attraction, then snaps off the surface at the point, where the long ranged restoring force of the cantilever becomes larger than the attractive force between sample and tip. This accounts for a visible hysteresis in force curves. The hysteresis shows the strength of the attractive forces between tip and sample (Radmacher et al., 1992c). No hysteresis can be seen in the force curve on our cells (*B*). With the given spring constant of the cantilever and the height resolution of our instrument the net force was estimated to be less than 60 pN. This finding suggests a long range repulsive force to balance the attractive van der Waals force. Also visible is a parallel shift in the approach and retract that can be understood as an effect of lateral forces (Hoh and Engel, 1993) and some nonlinearity in the contact portion of the curves due to sample elasticity (Tao et al., 1992; Weisenhorn et al., 1993).

The three effects—long range repulsive force, elastic behavior and high lateral forces—may be explained by the properties of the cell surface, especially of the glycocalix. A simple calculation shows that the elastic properties of the glycocalix can lead to a repulsive force of several tens of nN at a distance of a few nanometers. This force could balance the attractive van der Waals force. The glycocalix consists mainly of sugar chains that are grafted at one end to the cell membrane and are freely dangling at the other end. The glycocalix can be modeled, therefore, using the theory of grafted polymers (Alexander, 1977; Gennes, 1986). We neglect here that the glycocalix is charged. Because both glycocalix and tip are negatively charged the shielded Coulomb interaction would give rise to an additional repulsion. In this model we consider only entropic and steric contributions. A dense layer of grafted polymers (n segments with a segment length l, distance between grafting points s) builds up a so called brush of a thickness L

$$L = \frac{nl^{5/3}}{s^{2/3}}. \tag{1}$$

Two planar brushes in contact exhibit a decaying repulsive force, which can be approximated by an exponential function (Israelachvili, 1992). The interaction energy can be written as

$$W_{(d)} = \frac{aL}{\pi s^3} kT * e^{-\pi d/L}, \tag{2}$$

where d is the distance between the two surfaces, k is the Boltzmann constant, and T is the absolute temperature. a is a numerical constant and equals 100 in this case.

The interaction energy between two parallel plates can be transformed into the geometry of the AFM experiment-(a sphere touching a plane) by means of the Derjaguin approximation (Derjaguin, 1934)

$$F_{(d)} = W_{(d)} \pi R, \tag{3}$$

where R is the radius of the tip. This leads to the final equation for the force,

$$F_{(d)} = R \frac{aL}{s^3} kT * e^{-\pi d/L}. \tag{4}$$

We have to take into account that in the case of AFM, only one surface is coated by a grafted polymer (the cell), therefore replacing the thickness L of the brush by

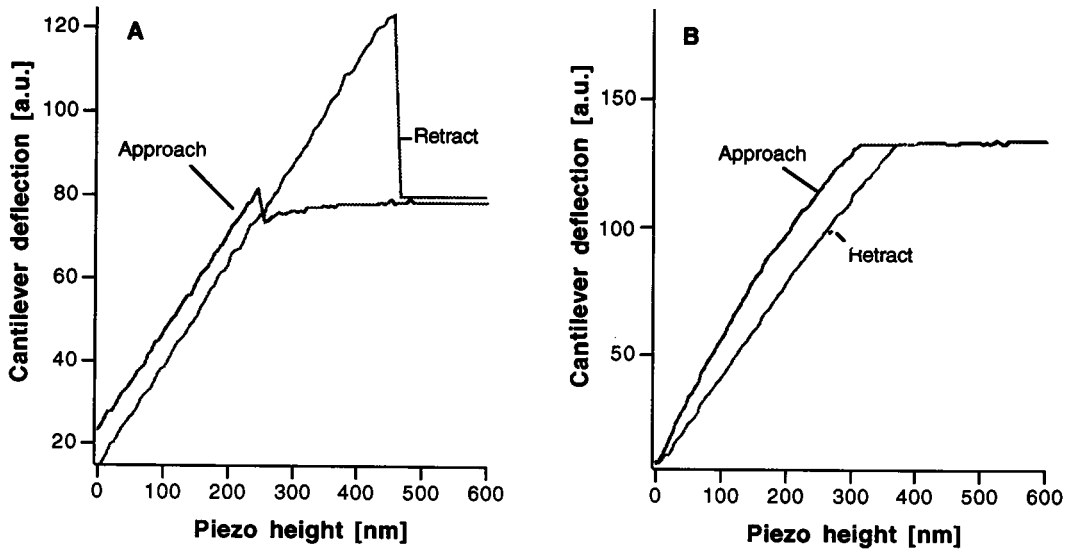

FIGURE 6 Force curves (*A*) on a glass slide and (*B*) on an activated living thrombocyte. Plotted is the deflection of the tip as a function of the sample position upon approach and retract. In *A* attractive forces lead to a clearly visible jump to contact during approach and a large hysteresis during retraction. These attractive forces are not visible on the cells in *B*. On the other hand, the two traces in the contact region in *B* are seperated and nonlinear, which can be explained by the effects of elastic and lateral forces.

its half value,

$$F_{(d)} = R\frac{aL}{2s^3}kT * e^{-2\pi d/L}. \quad (5)$$

This equation may be written in a simpler form,

$$F_{(d)} = F_0 * e^{-d/l_0} \quad (6)$$

using the abbreviations

$$F_0 = R\frac{aL}{2s^3}kT \qquad l_0 = L/2\pi. \quad (7)$$

With typical values for segment number (n = 20), segment length (l = 3 Å), mean distance between grafting points (s = 1 nm), and temperature (T = 300 K), the thickness of the (half) brush turns out to be $L/2$ = 3 nm, the decay length of the force becomes l_0 = 1 nm, and force at zero separation is F_0 = 45 nN. This model shows that the entropy elasticity of the glycocalix may give rise to a short range repulsive force between tip and cell surface, which is of the same size or even larger than the attractive van der Waals forces. This could explain why no net attractive forces were observed in the force curves on the thrombocytes (Fig. 6 *B*).

This additional repulsive interaction will lower the net force between tip and membrane, but it will, however, also limit the lateral resolution that can be obtained on cells (at least on cells with a glycocalix) when imaged at low forces: taking a typical value of 5 nN for the local van der Waals force, Eq. 6 leads to a equilibrium distance of about 10 nm between tip and cell surface. This value will then also be the lower limit for the lateral resolution. This limitation may be overcome by matching the repulsive potential of the glycocalix with attractive interactions, e.g., via charge interactions within the glycocalix. At present, however, the resolution is rather limited by the tip size.

The fact that the net local force between tip and membrane is repulsive implies that the external force that the tip exerts on the cell via the bent of the cantilever is balanced by the elasticity of the cytoskeleton and, to a minor degree, by the bending stiffness of the membrane (Duwe et al., 1990) (Fig. 1). Because both counter-forces are long range, the resulting minimum force is determined only by the accuracy of the height compensation. This accuracy depends not only on the properties of the instrument, but also on the parameters of the experiment like scan rate and height of the corrugations of the sample. Typical deviations in our experiments were about 1 nm. This gives a limiting force of about 30 pN, using cantilevers with a stiffness of 32 mN/m. Under realistic optimum conditions, future experiments with an accuracy of 1 Å and a cantilever stiffness of 10 mN/m may permit imaging forces as low as 1 pN, which is less than the force quanta in muscle contraction.

CONCLUDING REMARKS

Our results show that under certain conditions the AFM may noninvasively image dynamic processes in live cells under physiological conditions at an unparalleled resolution. We could record individual steps of the redistribution of cellular components such as transport of granula towards the cortex. We were able to follow the spreading of the membrane on the substrate and to resolve details of the cytoskeletal structures of live, unstained cells. These results indicate that the AFM, which is bridging the gap between light and electron microscopy, is applicable to a broad range of adherent cells. The finding that the net force between tip and thrombocyte membrane is repulsive implies that the lower force limit is, at present, only determined by the quality of the instrumentation.

Helpful discussions with W. Siess and E. Morgenstern and technical support from Digital Instruments are gratefully acknowledged. We thank R. Giles for carefully reading this manuscript.
This work was supported by the Deutsche Forschungsgemeinschaft.

REFERENCES

Alexander, S. 1977. Polymer adsorption on small spheres. A scaling description. *J. Phys.* 38:977–981.

Allen, D. A., L. R. Zacharski, S. T. Widirstky, R. Rosenstein, L. M. Zaitlin, and D. R. Burgess. 1979. Transformation and motolity of human platelets. *J. Cell Biol.* 83:126–142.

Behnke, O. 1976. Contractile systems in non-muscle tissues. Elsevier, Amsterdam.

Behnke, O., and D. Bray. 1988. Surface movements during spreading of blood platelets. *Eur. J. Cell Biol.* 46:207–216.

Binnig, G., C. F. Quate, and C. Gerber. 1986. Atomic force microscope. *Phys. Rev. Lett.* 56:930*a*. (Abstr.)

Cleveland, J. P., S. Manne, D. Bocek, and P. K. Hansma. 1993. A nondestructive method for determining the spring constant of cantilevers for scanning force microscopy. *Rev. Sci. Instrum.* 64:403–405.

Derjaguin, B. V. 1934. Untersuchungen über die Reibung und Adhäsion, IV. *Kolloid Z.* 69:155–164.

Duwe, H. P. J. Käs, and E. Sackmann. 1990. Bending elastic moduli of lipid bilayers: modulation by solutes. *J. Phys.* 51:945–962.

Evans, E. 1993. *Biophys. J.* New physical concepts for cell ameboid motion. 64:1306–1322.

Fritz, M., M. Radmacher, and H. E. Gaub. 1993. In Vitro activation of human platelets triggered and probed by SFM. *Exp. Cell Res.* 205:187–190.

Fritz, M., M. Radmacher, N. Petersen, and H. E. Gaub. 1994. Visualization and identification of intracellular structures by force modulation microscopy and drug induced degradation. *J. Vac. Sci. Techn.* In press.

Gennes, P. G. d. 1986. Polymers at an interface: a simplified view. *Adv. Coll. Interf. Sci.* 27:189–209.

Ginsberg, M. H., L. Taylor, and R. G. Painter. 1980. The mechanism of thrombin-induced platelet factor 4 secretion. *Blood.* 55:661*a* (Abstr.)

Häberle, W., J. K. H. Hörber, F. Ohnesorge, D. P. E. Smith, and G. Binnig. 1992. In situ investigations of living cells infected by viruses. *Ultramicroscopy.* 42:1161–1167.

Hartwig, J. H. 1992. Mechanisms of actin rearrangements mediating platelet activation. *J. Cell Biol.* 118:1421–1442.

Hartwig, J. H., and M. DeSisto. 1991. The cytoskeleton of the resting human blood platelet: structure of the membrane skeleton and its attachment to actin filaments. *J. Cell Biol.* 3:407–425.

Henderson, E., P. G. Haydon, and D. S. Sakaguchi. 1992. Actin filament dynamics in living glial cells imaged by AFM. *Science.* 257:1944–1946.

Hoh, J., and A. Engel. 1993. Friction effects in force curves. *Langmuir.* 9:3310–3312.

Holmsen, H. 1984. Platelets—Cellular Response Mechanisms, and Their Biological Significance. A. Rotman, F. A. Meyer, C. Gitler, and A. Silberberg, editors. John Wiley & Sons, Rehovot, Israel. 249–263.

Israelachvili, J. N. 1992. Intermolecular, and Surface Forces. Academic Press, London.

Keller, D. L. Chang, K. Luo, S. Singh, and M. Yorganciogla. 1992. Scanning force microscopy of cells and membrane proteins. *Proc. SPIE.* 1639:91–101.

Loftus, C. J., J. Choate, and R. M. Albrecht. 1984. Platelet activation and cytoskeletal reorganisation: high voltage electron microscopic examination of intact and triton-extracted whole mounts. *J. Cell Biol.* 98: 2019–2025.

Morgenstern, E., and A. Kho. 1977. Morphometric measurements on blood platelets: changes in the structure of platelets during pseudopodia formation and aggregation. *Eur. J. Cell Biol.* 15:233–249.

Morgenstern, E., U. Korell, and J. Richter. 1984. Platelets and fibrin strands during clot retraction. *Thrombosis Res.* 33:617–623.

Morgenstern, E., K. Neumann, and H. Patscheke. 1987. The exocytosis of human blood platelets. A fast freezing and freeze-substitution analysis. *Eur. J. Cell Biol.* 43:273–282.

Nachmias, V. T. 1980. Cytoskeleton of human platelets at rest and after spreading. *J. Cell Biol.* 86:795–802.

Painter, R. G., and M. H. Ginsberg. 1981. Redistribution of platelet actin and myosin in association with thrombin induced secretion. *Fed. Proc.* 40:212–213.

Pollard, T. D., K. Fujiwara, R. Handin, and G. Weiss. 1977. Contractile proteins in platelet activation and contraction. *Ann. N. Y. Acad. Sci.* 283: 218–236.

Putman, C. A. J., K. O. van der Werf, B. G. de Grooth, N. F. van Hulst, J. Greve, and P. K. Hansma. 1992. A new imaging mode in Atomic Force Microscopy based on the error signal. *Proc. SPIE.* 1639:198–204.

Radmacher, M., K. Eberle, and H. E. Gaub. 1992a. An AFM with integrated micro fluorescence optics—design and performance. *Ultramicroscopy.* 42:968–972.

Radmacher, M., R. W. Tillmann, M. Fritz, and H. E. Gaub. 1992b. From molecules to cells—imaging soft samples with the AFM. *Science.* 257: 1900–1905.

Radmacher, M., R. M. Zimmermann, and H. E. Gaub. 1992c. The Structure, and Conformation of Amphiphilic Membranes. R. Lipowski, D. Richter, and K. Kremer, editors. Springer, Berlin. 24–29.

Sixma, J. J., A. van den Berg, B. Jockusch, and J. Hartwig. 1989. Immunoelectron microscopic lokalisation of actin, alpha-actinin, actin-binding protein and myosin in resting and activated human blood platelets. *Eur. J. Cell Biol.* 48:271–281.

Stenberg, P. E., M. A. Shuman, S. P. Levine, and D. F. Bainton. 1984. Redistribution of alpha-granules and their contents in thrombin-stimulated platelets. *J. Cell Biol.* 98:748–760.

Tao, N. J., N. M. Lindsay, and S. Lees. 1992. Measuring the microelastic properties of biological materials. *Biophys. J.* 63:1165–1169.

Weisenhorn, A. L., M. Khorsandi, S. Kasas, V. Gotozos, M. R. Celio, and H. J. Butt. 1993. Deformation and height anomaly of soft surfaces studied with the AFM. *Nanotechnology.* 4:106–113.

White, J. G. 1983. Methods in Haematology. Series 8. Churchill Livingstone, New York.

White, J. G. 1987. The secretory pathway of bovine platelets. *Blood.* 69:878–885.

White, J. G., and M. Krumwiede. 1987. Further studies of the secretory pathway in thrombin stimulated human platelets. *Blood.* 69:1196–1203.

Zucker-Franklin, D., K. A. Benson, and K. M. Meyers. 1985. Absence of a surface-connected canalicular system in bovine platelets. *Blood.* 65: 241*a*. (Abstr.)